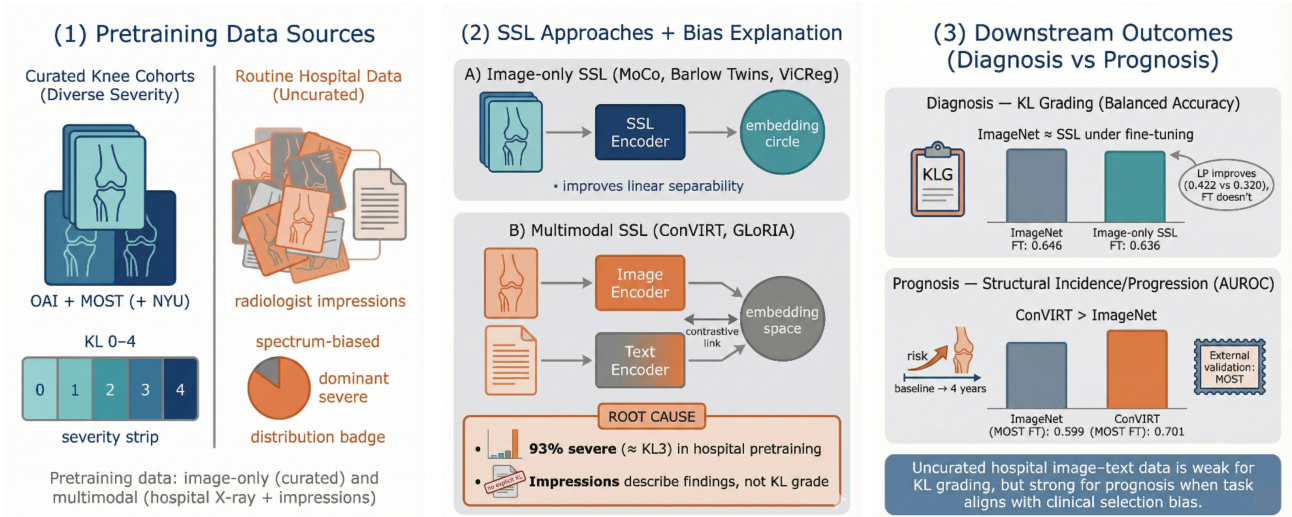


Graphical Abstract

Self-Supervised Learning for Knee Osteoarthritis: Diagnostic Limitations and Prognostic Value of Uncurated Hospital Data

Haresh Rengaraj Rajamohan, Yuxuan Chen, Kyunghyun Cho, Cem M. Deniz



Highlights

Self-Supervised Learning for Knee Osteoarthritis: Diagnostic Limitations and Prognostic Value of Uncurated Hospital Data

Haresh Rengaraj Rajamohan, Yuxuan Chen, Kyunghyun Cho, Cem M. Deniz

- Image-only self-supervised learning improves linear probing (0.422 vs. 0.320 Acc) but yields no advantage over ImageNet pretraining for knee diagnosis (0.636 vs. 0.646 Acc) and chest disease classification tasks under rigorous fine-tuning.
- Multimodal pretraining on uncurated hospital radiographs and text impression fails to improve diagnostic grading (ConVIRT 0.627 vs. ImageNet 0.646 Acc) due to severe spectrum bias toward advanced disease (93% KL Grade 3).
- The inherent selection bias in uncurated hospital data paradoxically benefits prognostic modeling, enabling multimodal learning to significantly outperform ImageNet on structural progression prediction (AUROC 0.701 vs. 0.599 on external validation).

Self-Supervised Learning for Knee Osteoarthritis: Diagnostic Limitations and Prognostic Value of Uncurated Hospital Data

Haresh Rengaraj Rajamohan^{a,*}, Yuxuan Chen^d, Kyunghyun Cho^a and Cem M. Deniz^{c,b}

^aCenter for Data Science, New York University, New York, 10011, NY, United States

^bBernard and Irene Schwartz Center for Biomedical Imaging, New York University Langone Health, New York, 10016, NY, USA

^cDepartment of Radiology, New York University Langone Health, New York, 10016, NY, USA

^dPerlmutter Cancer Center, New York University Langone Health, New York, 10016, NY, USA

ARTICLE INFO

Keywords:

Knee Osteoarthritis
Pretraining
Self-Supervised Learning
Multimodal Learning
Prognosis
Deep Learning
Contrastive Learning

ABSTRACT

This study assesses whether self-supervised learning (SSL) improves knee osteoarthritis (OA) modeling for diagnosis and prognosis relative to ImageNet-pretrained initialization. We compared (i) image-only SSL pretrained on knee radiographs from the OAI, MOST, and NYU cohorts, and (ii) multimodal image-text SSL pretrained on uncurated hospital knee radiographs paired with radiologist impressions. For diagnostic Kellgren-Lawrence (KL) grade prediction, SSL offered mixed results. While image-only SSL improved accuracy during linear probing (frozen encoder), it did not outperform ImageNet pretraining during full fine-tuning. Similarly, multimodal SSL failed to improve grading performance. We attribute this to severe bias in the uncurated hospital pretraining corpus (93% estimated KL grade 3), which limited alignment with the balanced diagnostic task. In contrast, this same multimodal initialization significantly improved prognostic modeling. It outperformed ImageNet baselines in predicting 4-year structural incidence and progression, including on external validation (MOST AUROC: 0.701 vs. 0.599 at 10% labeled data). Overall, while uncurated hospital image-text data may be ineffective for learning diagnosis due to severity bias, it provides a strong signal for prognostic modeling when the downstream task aligns with pretraining data distribution.

1. Introduction

Knee Osteoarthritis (OA) is a progressive, debilitating joint disorder and a leading cause of disability worldwide. Its gradual onset and potential for irreversible structural damage make early intervention crucial for optimizing patient outcomes and reducing long-term healthcare costs [1]. However, the clinical management of knee OA faces a critical bottleneck: accurately predicting prognosis. Specifically, identifying which patients will experience rapid structural deterioration remains a significant challenge. Reliable prognostic models are essential for guiding timely behavioral interventions and optimizing patient selection for clinical trials, yet their development is hindered by the scarcity of labeled longitudinal data.

Deep learning (DL) has fundamentally transformed medical image analysis, demonstrating diagnostic performance comparable to human experts across domains ranging from diabetic retinopathy detection to dermatological lesion classification [2, 3, 4, 5]. DL has also shown immense promise for automating knee OA assessment. Foundational works by Tiulpin et al. [6], Zhang et al. [7] successfully leveraged convolutional neural networks (CNNs) to automate disease severity grading (Kellgren-Lawrence [KL] grading [8]) from plain radiographs. Building on this diagnostic success, recent research has pivoted toward complex prognostic tasks, such as predicting total knee replacement (TKR) risk

or forecasting disease progression using knee radiographs and MRIs [9, 10, 11, 12, 13]. However, a fundamental disparity exists in data availability. While diagnostic datasets can be assembled from independent one-time imaging exams across patients, prognostic datasets require years of continuous patient follow-up to capture disease trajectories.

To address label scarcity, self-supervised learning (SSL) has emerged as a transformative paradigm in deep learning. By defining pretext tasks, such as instance discrimination or image-text matching, SSL allows models to learn robust representations from vast repositories of unlabeled data. In the natural image domain, contrastive methods (e.g., SimCLR, MoCo) and non-contrastive methods (e.g., Barlow Twins, ViCReg, DINO) have demonstrated that SSL pretraining can rival or exceed supervised pretraining on ImageNet classification, particularly in low-labeled data regimes [14, 15, 16, 17, 18]. Furthermore, multimodal approaches like CLIP [19], which leverage image-caption pairs, have pushed the boundaries of zero-shot transfer and downstream classification performance.

These advancements are particularly relevant in the medical domain, where hospitals generate vast volumes of unlabeled scans. Pioneering works have adapted SSL to tasks ranging from chest X-ray interpretation to dermatology, often demonstrating that “in-domain” pretraining yields superior downstream performance compared to standard ImageNet [20] initialization [21, 22, 23, 24, 25]. A key open question is whether in-domain SSL using routine-care knee radiographs (with or without paired reports) provides reliable gains over ImageNet for both cross-sectional severity grading and longitudinal prognosis.

*Corresponding author

✉ hrr288@nyu.edu (H.R. Rajamohan); Yuxuan.Chen@nyulangone.org (Y. Chen); kc119@nyu.edu (K. Cho); cem.deniz@nyulangone.org (C.M. Deniz)

ORCID(s):

However, the application of SSL to knee OA faces a practical dilemma regarding data availability and distribution. In routine-care hospital data, standardized KL grades are typically not recorded, and even when proxy KL labels can be obtained, the radiograph distribution is strongly spectrum-biased because imaging is ordered for symptomatic patients. As a result, learning a general-purpose KL grader requires curated cohorts with broad severity coverage (e.g., OAI and MOST), which are expensive to collect and limited in scale. In contrast, radiologist impressions are produced as part of standard clinical workflow and are available at hospital scale. This accessibility motivates multimodal SSL as a practical alternative for representation learning, despite the inherent spectrum bias of the underlying data.

In this study, we analyze when SSL pretraining improves knee OA modeling under realistic limited labeled data fine-tuning protocols. First, we show that standard image-only SSL strategies, even when trained on diverse in-domain knee radiographs (OAI and MOST datasets), do not consistently outperform ImageNet initialization for KL grading under fine-tuning, despite improved linear probing. Notably, this limitation was not unique to knee OA; we observed similar stagnation when replicating these image-only experiments on chest x-rays from NIH chest radiograph dataset. Second, we evaluate multimodal contrastive pretraining (ConVIRT, GLoRIA) on routine-care hospital knee radiographs paired with impression text. While we observed that ConVIRT multimodal pretraining reproduces expected gains in chest radiography on Chexpert, it does not improve KL grading for knee OA. We attribute this discrepancy to task-data mismatch: the hospital knee corpus is heavily enriched for symptomatic OA, yielding an extremely skewed severity spectrum (93% pseudo-labeled $KL=3$), and impression text also never encodes the KL grade explicitly, limiting supervision for learning KL decision boundaries unlike chest datasets.

Finally, we test whether multimodal pretraining is better matched to prognostic endpoints that require discrimination among similarly diseased knees. We evaluate 4-year structural incidence and progression prediction on OAI and external validation on MOST, comparing multimodal SSL against ImageNet and an upper-bound supervised initialization pretrained on expert KL labels from OAI. We find that multimodal SSL significantly improves prognosis performance across all labeled-data fractions and enhances discrimination of progressors within each KL strata, indicating robust performance improvements. Together, these findings highlight that routine-care image-text data may be poorly suited for learning general OA severity graders, yet can provide a scalable and effective signal for prognostic modeling when aligned with the downstream task.

2. Materials and Methods

2.1. Data Sources

This retrospective study utilized data from three independent sources: the Osteoarthritis Initiative (OAI), the Multicenter Osteoarthritis Study (MOST), and a dataset from NYU Langone Health.

The **Osteoarthritis Initiative (OAI)** is a multicenter, prospective observational study of knee OA [26]. We obtained bilateral knee radiographs and clinical data spanning baseline to 108-month follow-up. The OAI dataset served as the primary source for downstream evaluation for diagnosis and prognosis tasks.

The **Multicenter Osteoarthritis Study (MOST)** is a longitudinal observational study of individuals with or at high risk of knee OA [27] evaluated at baseline to 168-month follow-up. MOST data was utilized as an external validation cohort to assess the generalizability of the diagnosis and prognosis models.

NYU Langone Health Dataset: This dataset represents uncurated routine clinical data acquired from a tertiary care center. Retrospective data was collected from the electronic medical records and PACS of NYU Langone Health spanning January 1, 2011, to September 1, 2017 (IRB No. 117-01339). The cohort included patients who underwent knee radiography or MRI and carried a clinical diagnosis of primary knee osteoarthritis; patients with incomplete demographic data (age, sex, BMI, ethnicity) were excluded. This dataset was fully de-identified and utilized exclusively for self-supervised pretraining.

For the chest experiments, we utilized MIMIC-CXR [28], CheXpert [4], and NIH Chest X-ray 14 [29] datasets. The multimodal pretraining was performed using image-text pairs from MIMIC-CXR and downstream task evaluation was performed on CheXpert. For the image only self-supervised training, NIH Chest X-ray 14 was used for both pretraining and downstream evaluation.

2.2. Data Partitioning and Preprocessing

2.2.1. Pretraining Datasets

To evaluate the impact of data distribution, we curated two distinct pretraining datasets:

- **Image-Only Pretraining Dataset ($D_{SSL-Image}$):** A large-scale, diverse dataset comprising 57,325 extracted bilateral knee joint radiographs from OAI, MOST, and NYU. To prevent data leakage, patients assigned to the validation or test sets of the diagnosis and prognosis downstream tasks (OAI/MOST) were strictly excluded.
- **Multimodal Pretraining Dataset ($D_{SSL-Multi}$):** A dataset comprising 84,294 pairs of knee radiographs and free-text radiology impressions exclusively from NYU Langone Health. Unlike $D_{SSL-Image}$, this dataset reflects the natural selection bias of a tertiary care center. The acquisition protocols were heavily skewed

toward osteoarthritis assessment, with the vast majority of exams consisting of weight-bearing antero-posterior (AP) or posteroanterior (PA) flexion views, accompanied by lateral and patellar (sunrise) projections. Bilateral studies dominated the cohort, though unilateral and portable bedside acquisitions were also present. Analysis of the disease distribution in bilateral knee joints (inferred via a supervised proxy model) estimated that approximately 93% of this cohort represents KL Grade 3.

2.2.2. Image and Text Preprocessing

For all datasets, knee joints were localized and cropped from bilateral radiographs. We utilized a ResNet-based localization model trained to directly regress bounding box coordinates for the knee joints [7]. Based on these predictions, regions of interest (ROIs) of size 1024×1024 pixels were extracted. These ROIs were subsequently resized to 256×256 pixels, followed by random cropping to 224×224 pixels and normalization during training. For multimodal learning, text impressions were extracted from radiology reports. We deidentified and removed PHI from the text using [30], applied standard text cleaning (lowercasing, removal of special characters) and tokenization using the WordPiece tokenizer with a maximum sequence length of 512 tokens.

2.3. Model Development and Pretraining

We utilized a ResNet34 [31] backbone for all the knee experiments similar to previous works [7] (ResNet50 for the Chest experiments). We implemented two categories of self-supervised learning (SSL):

2.3.1. Image-Only SSL

We trained models on $D_{SSL-Image}$ using four approaches:

- **MoCo:** Utilized a momentum encoder and a queue of negative samples to maximize similarity between augmented views of the same image [15].
- **Barlow Twins:** Minimized the cross-correlation matrix difference between distorted views to identity [16] without requiring negative pairs.
- **ViCReg:** Enforced variance, invariance, and covariance regularization without requiring negative pairs [17].
- **CNN-JEPA:** A non-contrastive, predictive SSL objective that learns representations by predicting latent embeddings of masked/held-out regions from context, encouraging invariant and information-rich features without explicit negative pairs [32, 33].

2.3.2. Multimodal SSL

We trained models on $D_{SSL-Multi}$ using image-text pairs:

- **ConVIRT:** Optimized a bidirectional contrastive loss ($L_{InfoNCE}$) to maximize the similarity between the

image embedding and its corresponding text embedding relative to other pairs in the batch [23].

- **GLORIA:** Utilized a global-local attention mechanism to align specific image sub-regions with word-level text features, hypothesized to capture localized pathology [24].

2.4. Downstream Evaluation Tasks

2.4.1. Knee Osteoarthritis (OA)

We evaluated the models on two primary clinical tasks using the OAI and MOST datasets:

- **Diagnosis:** Classification based on Kellgren-Lawrence Grade (KLG) [8] – A severity scale (0-4) assigned by radiologists based on radiographic features including joint space narrowing, bone spurs, and sclerosis.
- **Prognosis:** Prediction of disease worsening over a 4-year horizon [34], defined as:
 - *Structural Incidence* for early-stage OA (KLG 0-1): Progression to $KLG \geq 2$ or undergoing a Total Knee Replacement (TKR).
 - *Structural Progression* for radiographic OA ($KLG \geq 2$): An increase in KLG or undergoing a TKR.

2.4.2. Chest Radiography (Control Experiments)

To validate the methodology in a domain where SSL is established, we conducted two independent control experiments with distinct downstream evaluation tasks:

- **Image-Only SSL:** We pretrained and fine-tuned image-only encoders (MoCo, ViCReg) using the **NIH Chest X-ray 14** dataset [29]. The downstream task was multi-label classification of the 14 standard thoracic pathologies (e.g., Pneumothorax, Effusion) defined in the dataset. This assessed whether pixel-only pretraining offers gains when the pretraining and downstream data distributions are identical.
- **Multimodal SSL:** We pretrained multimodal encoders (ConVIRT) using the image-text pairs from the **MIMIC-CXR** dataset [28]. These models were then fine-tuned on the **CheXpert** dataset [4] for the standard 5-disease classification task (Atelectasis, Cardiomegaly, Consolidation, Edema, and Pleural Effusion). This served to validate our multimodal implementation against established benchmarks.

2.5. Experimental Pipeline and Evaluation Protocol

The overall experimental workflow employed in this study is illustrated in Figure 1. The process is divided into two primary stages: (1) Self-supervised pretraining on unlabeled data (D_{pret}), and (2) Supervised fine-tuning on downstream task data (D_{task}).

Table 1

Patient Characteristics in Structural Progression Cohorts (OAI and MOST). Data are presented as mean \pm standard deviation where applicable. BMI = Body Mass Index.

Dataset	Parameters	Men		Women		
		Patients	Controls	Patients	Controls	
OAI	No. of patients	216	707	355	970	
	No. of scans	241	917	421	1348	
	Mean age (y)	62.3 \pm 9.0	62.1 \pm 9.3	63.7 \pm 8.2	62.5 \pm 8.9	
	Mean height (m)	1.8 \pm 0.1	1.8 \pm 0.1	1.6 \pm 0.1	1.6 \pm 0.1	
	Mean weight (kg)	93.1 \pm 14.3	91.7 \pm 14.4	80.8 \pm 14.8	78.2 \pm 14.5	
	Mean BMI (kg/m ²)	30.1 \pm 4.0	29.3 \pm 4.0	30.6 \pm 5.2	29.6 \pm 5.3	
	<i>Ethnicity</i>					
	White	184	595	253	721	
	Black	26	97	90	230	
	Asian	2	4	3	5	
Other nonwhite	4	11	9	14		
MOST	No. of patients	203	231	359	386	
	No. of scans	231	282	427	495	
	Mean age (y)	62.8 \pm 8.5	63.2 \pm 8.4	64.2 \pm 7.6	63.5 \pm 7.3	
	Mean height (m)	1.8 \pm 0.1	1.8 \pm 0.1	1.6 \pm 0.1	1.6 \pm 0.1	
	Mean weight (kg)	100.9 \pm 19.8	98.3 \pm 17.8	86.3 \pm 18.5	85.0 \pm 18.2	
	Mean BMI (kg/m ²)	32.0 \pm 5.8	31.1 \pm 5.4	32.7 \pm 6.8	31.9 \pm 6.6	
	<i>Ethnicity</i>					
	White	177	197	288	302	
	Black	22	32	63	82	
	Other	4	2	8	2	

2.5.1. Realistic Low-Data Evaluation

A critical aspect of our methodology is the rigorous handling of low-data regimes during fine-tuning. As shown in the "Sample partial data" block of Figure 1, when evaluating performance at specific data fractions (e.g., 1%, 5%, 10%), we sample that fraction proportionally from **both** the available training (D_{task}) and validation (D_{FT}^{val}) pools.

This approach contrasts with common practices in prior medical SSL literature (e.g., some chest X-ray studies) [21, 23], where models trained on tiny fractions of data are often tuned using larger, fixed-size validation sets. We argue that such protocols are unrealistic; in real-world scenarios where training labels are scarce, labeled validation data is equally scarce. By constraining the validation set size proportionally, our protocol provides a more stringent and realistic assessment of a model's true data efficiency.

2.6. Control Experiments: Investigating Image-Only Limitations

To rigorously investigate why image-only SSL might fail in the medical domain, we conducted specific control studies disentangling dataset size and domain complexity.

2.6.1. Effect of Pretraining Dataset Size

We hypothesized that the performance gap between Medical SSL and ImageNet transfer might stem from the sheer size of pretraining dataset (ImageNet - 1.2M images). To test this, we conducted two scaling experiments:

- **Natural Image Scaling:** We created random subsets of ImageNet matching the scale of our medical

datasets (6k, 10k, 25k, 40k, 58k images). We pre-trained MoCo encoders on these subsets and evaluated their downstream performance on KLG diagnosis.

- **In-Domain Scaling:** We pretrained encoders on random subsets of our Knee dataset (6k to 58k) to see if a larger in-domain dataset scales performance.

A positive relationship between pretraining scale and downstream performance would suggest that the current knee pretraining dataset is of insufficient size. Conversely, a performance plateau would indicate that the limiting factor is the intrinsic information content of the data or downstream task complexity, rather than dataset size.

2.6.2. Effect of Domain Complexity

To test if the performance limitations of SSL lies in the medical images themselves (e.g., subtle grayscale texture vs. distinct natural objects in focus), we utilized **Imagenette**, a subset of 10 easily discriminable ImageNet classes. We pretrained encoders using SSL on progressively larger subsets of the ImageNet training set and evaluated them on Imagenette classification. This object-centric control isolates the effect of natural-image pretraining scale under a simpler visual recognition task, and serves as a sanity check that our SSL training and evaluation pipeline behaves as expected before applying the same methodology to knee radiographs.

2.7. Evaluation Setup

For the downstream tasks, we evaluated performance using both **Linear Probing (LP)** (frozen backbone) and

Table 2

Patient Characteristics in Structural Incidence Cohorts (OAI and MOST). Data are presented as mean \pm standard deviation where applicable.

Dataset	Parameters	Men		Women		
		Patients	Controls	Patients	Controls	
OAI	No. of patients	149	1103	271	1336	
	No. of scans	160	1737	296	2171	
	Mean age (y)	61.0 \pm 8.7	59.6 \pm 9.4	60.3 \pm 8.6	60.5 \pm 9.0	
	Mean height (m)	1.8 \pm 0.1	1.8 \pm 0.1	1.6 \pm 0.1	1.6 \pm 0.1	
	Mean weight (kg)	91.0 \pm 14.9	91.0 \pm 14.9	77.2 \pm 14.2	71.3 \pm 13.3	
	Mean BMI (kg/m ²)	29.1 \pm 4.1	28.1 \pm 3.8	29.3 \pm 4.8	27.1 \pm 4.8	
	<i>Ethnicity</i>					
	White	133	975	208	1121	
	Black	13	110	56	180	
	Asian	1	4	4	13	
Other nonwhite	2	12	2	21		
MOST	No. of patients	179	600	326	795	
	No. of scans	196	945	371	1304	
	Mean age (y)	61.3 \pm 7.8	60.6 \pm 7.8	62.4 \pm 8.0	61.1 \pm 7.7	
	Mean height (m)	1.8 \pm 0.1	1.8 \pm 0.1	1.6 \pm 0.1	1.6 \pm 0.1	
	Mean weight (kg)	99.8 \pm 17.1	93.7 \pm 15.1	82.6 \pm 15.6	77.4 \pm 14.1	
	Mean BMI (kg/m ²)	31.3 \pm 5.3	29.6 \pm 4.5	30.9 \pm 5.9	28.8 \pm 5.2	
	<i>Ethnicity</i>					
	White	157	573	270	694	
	Black	19	73	50	89	
	Other	3	10	3	12	

Full Fine-Tuning (FT). As illustrated in Figure 1, to ensure robust comparisons:

- **Bayesian Hyperparameter Tuning:** We utilized the **Optuna** framework [35] with Tree-structured Parzen Estimators (TPE) to optimize hyperparameters like learning rate, weight decay, optimizer and scheduler for every method-dataset-fraction combination on the proportional validation sets.
- **Model Selection and Seeds:** To ensure statistical robustness, experiments were repeated across 10 independent random seeds. Crucially, the random subsampling of training and validation sets was distinct for each seed, ensuring that reported metrics reflect performance stability across different data distributions. For each run, the final model checkpoint was selected based on the optimal metric achieved on the validation set.
- **Metrics:** Performance is reported as Balanced Accuracy for KLG diagnosis. For Knee OA prognosis, performance is reported as the standard Area Under the ROC Curve (AUROC). For the multi-label Chest radiography tasks, we report the Macro-averaged AUROC. All results represent the mean and standard deviation across multiple independent random seeds evaluated on the held-out test set (D_{FT}^{test}).

3. Results

3.1. Image-Only SSL Fails to Outperform ImageNet pretrained Baseline

We first investigated whether large-scale in-domain pre-training on radiographs alone ($D_{SSL-Image}$) could outperform standard transfer learning. Table 3 summarizes the performance of four image-only SSL methods (MoCo, Barlow Twins, ViCReg, and CNN-JEPA) compared to ImageNet initialization and random initialization on the downstream task of KLG diagnosis.

Lack of Advantage over ImageNet: Both ImageNet and in-domain SSL substantially outperform random initialization, confirming that pretraining is beneficial in the low-label regime. However, contrary to the “in-domain is better” hypothesis, ImageNet remains a consistently strong baseline: under full fine-tuning (FT) at 10% labeled data, ImageNet achieves 0.646, marginally outperforming the best in-domain method (MoCo: 0.636).

Linear Probing vs. Fine-Tuning: While in-domain SSL yielded higher Linear Probing (LP) accuracy than ImageNet (e.g., MoCo LP: 0.422 vs. ImageNet LP: 0.320 at 10% data) consistently, this advantage disappeared with fine-tuning. We observe the same overall pattern under additional image-only controls (mixed-domain diversity and MAE pretraining; Appendix A–B).

Table 3

Image-Only SSL vs. ImageNet for Knee OA Diagnosis. KLG prediction performance (Balanced Accuracy) on OAI test set. Note that ImageNet pretraining (Imgnnet-pret) consistently rivals or beats in-domain SSL under fine-tuning.

Pretraining Approach	1% Data		5% Data		10% Data	
	FT	LP	FT	LP	FT	LP
Random	0.397 (0.042)	0.200	0.555 (0.011)	0.200	0.619 (0.015)	0.200
Imgnnet-pret	0.483 (0.040)	0.263	0.613 (0.014)	0.308	0.646 (0.009)	0.320
MoCo (Knee)	0.475 (0.050)	0.368	0.606 (0.010)	0.411	0.636 (0.012)	0.422
Barlow (Knee)	0.425 (0.063)	0.324	0.589 (0.018)	0.355	0.620 (0.010)	0.358
ViCReg (Knee)	0.471 (0.048)	0.336	0.585 (0.018)	0.374	0.635 (0.007)	0.373
CNN-JEPA (Knee)	0.476 (0.043)	0.253	0.606 (0.015)	0.33	0.631 (0.009)	0.375

3.2. Analysis: Data scale and task complexity

3.2.1. The Data Scale Hypothesis

We first tested if the performance limitations stemmed from insufficient pretraining data by analyzing the scaling laws for both natural and in-domain images.

Result: As shown in Figures 2 and 3, we observed a distinct performance plateau in both scenarios.

- **ImageNet Scaling:** Reducing ImageNet size from Full (1.2M) to 58k resulted in negligible degradation (e.g., 0.648 vs. 0.627 at 10% data), suggesting that vast scale is not required for the KLG task.
- **Knee Scaling:** More critically, increasing in-domain pretraining data from 6k to 58k also yielded minimal gains (e.g., 0.627 vs. 0.636 at 10% data).

Together, these results confirm that the bottleneck is not the *quantity* of pretraining data.

3.2.2. The Task Complexity Hypothesis

Having ruled out dataset size as the primary bottleneck, we investigated whether the limitation lay in the inherent *complexity* of the downstream task itself.

In stark contrast to the stagnant results on the Knee dataset, Figure 4 demonstrates strong, predictable scaling on Imagenette. The model achieves high accuracy (0.844) with just 10% labeled data, and the performance improves consistently as the size of the pretraining data increases showing the expected scaling behavior.

Additional controls (Appendix). We further tested whether increasing visual diversity via mixed-domain medical pretraining (Knee+Chest) or cross-domain transfer could overcome the image-only bottleneck; these analyses did not yield consistent gains over ImageNet or in-domain knee pretraining (Appendix A). We also evaluated a generative image-only SSL approach (MAE) and observed similar diagnostic stagnation despite successful reconstructions (Appendix B).

3.3. Cross-Domain Validation: Image-Only vs. Multimodal SSL

To confirm that this limitation is not unique to Knee OA, we replicated experiments on Chest Radiography.

Image-Only SSL Results: Consistent with our Knee results, image-only SSL (MoCo, ViCReg) on Chest X-rays failed to outperform ImageNet initialization (Table 4).

Table 4

Image-Only SSL Failure on Chest X-rays. Macro AUROC on NIH Chest X-ray 14. Similar to Knee OA, pixel-only pretraining does not consistently beat ImageNet.

Pretraining	1% (FT)	5% (FT)	10% (FT)
Imgnnet-pret	0.619 (0.013)	0.699 (0.011)	0.732 (0.009)
Chest MoCo	0.572 (0.015)	0.646 (0.012)	0.680 (0.004)
Chest ViCReg	0.558 (0.018)	0.668 (0.006)	0.699 (0.004)

Multimodal SSL Results: However, when we introduced text reports (Multimodal SSL) on the Chest dataset, we observed a significant performance jump. As shown in Table 5, ConVIRT pretrained on CheXpert significantly outperformed ImageNet (e.g., 83.5 vs 72.6 LP at 1% data). This validates that our multimodal implementation is correct and effective when the data distribution supports it.

3.4. The Knee Diagnosis Paradox and Root Cause Analysis

Despite the success in Chest X-rays, applying the same Multimodal pipeline (ConVIRT, GLORIA) to the Knee dataset yielded unexpected results for Diagnosis (KL Prediction).

Failure at Diagnosis: As shown in Table 6, multimodal pretraining substantially improves linear-probe performance over both ImageNet and image-only SSL (e.g., ConVIRT LP: 0.531 vs ImageNet LP: 0.32 at 10% data), indicating that the pretrained representation captures disease-associated features present in the hospital cohort. However, these gains do not consistently translate to improved KL grading under fine-tuning (ConVIRT FT: 0.627 vs ImageNet FT: 0.646), suggesting a mismatch between the pretraining signal (disease-enriched impressions) and the downstream diagnostic decision boundaries required for KLG prediction.

Root Cause - Selection Bias: We hypothesized that this failure stemmed from the specific inclusion criteria of the pretraining cohort. Since the NYU dataset consists of patients with a clinical diagnosis of osteoarthritis at a tertiary care center, we expected a skew toward symptomatic, advanced disease. We inferred labels for the unlabeled hospital pretraining set using a supervised proxy model trained on the OAI dataset. Figure 5 reveals a severe selection bias: **93.0% of the pretraining data was estimated to be KL Grade 3**

Table 5

Multimodal SSL Success on Chest X-rays (Control Experiment). When paired with reports, SSL (ConVIRT) significantly outperforms ImageNet (macro AUROC), proving the pipeline works in a standard setting.

Approach	1% Data		5% Data		10% Data	
	LP	FT	LP	FT	LP	FT
Imgnet	72.6 (0.8)	75.9 (1.8)	76.9 (0.9)	82.8 (1.8)	78.5 (0.7)	83.8 (1.4)
ConVIRT	83.5 (0.7)	79.5 (3.4)	85.1 (0.3)	85.7 (1.1)	85.5 (0.3)	86.2 (0.7)

Table 6

Multimodal SSL Results for Knee Diagnosis. Balanced Accuracy on OAI. Unlike Chest, Multimodal SSL fails to improve Diagnosis due to the lack of healthy controls in the pretraining data.

Approach	1% Data		5% Data		10% Data	
	FT	LP	FT	LP	FT	LP
Imgnet	0.483	0.268	0.613	0.308	0.646	0.320
ConVIRT	0.570	0.455	0.619	0.520	0.627	0.531
GLORIA	0.400	0.411	0.558	0.463	0.589	0.482

(**Advanced OA**) further confirmed by the inclusion criteria which included patients with Knee OA diagnosis. Unlike the balanced screening data in Chest X-rays, the hospital knee data lacks the healthy controls necessary to learn decision boundaries for diagnosis.

3.5. Knee OA Prognosis Results

While the skewed distribution hindered diagnosis, we hypothesized it might be optimal for Prognosis, which requires differentiating between similarly diseased knees to predict progression.

Superior Prognostic Performance: Table 7 presents performance on Structural Progression. Both multimodal approaches (ConVIRT, GLORIA) consistently improve AUROC over ImageNet and image-only SSL across label fractions, indicating that paired image–text pretraining is particularly well matched to prognostic discrimination among diseased knees. ConVIRT yields the strongest gains, approaching the **KL-Supervised Baseline** (pretrained on radiologist KL grades).

4. Discussion

In this study, we evaluated the utility of self-supervised learning (SSL) for knee osteoarthritis (OA) across diagnosis to longitudinal prognosis. Our results challenge the prevailing assumption in medical imaging that in-domain pretraining on unlabeled medical scans invariably yields superior representations compared to transfer learning from natural images (ImageNet). We further identify a critical dichotomy: while uncurated hospital radiographs and radiologist text impressions fail to improve diagnostic severity grading due to severe selection bias, this same bias renders it highly effective for the more challenging task of prognosis.

A primary finding of this work is the stagnation of image-only SSL (MoCo, Barlow Twins, ViCReg) for knee

OA diagnosis. We observed a consistent discrepancy between Linear Probing (LP) and Fine-Tuning (FT) performance. In Linear Probing, in-domain SSL consistently outperformed ImageNet initialization. This confirms that in-domain pretraining successfully learned radiographic representations that are linearly separable and more semantically aligned with the downstream task than generic natural image features.

However, this advantage vanished under full Fine-Tuning, where ImageNet initialization matched or slightly exceeded the performance of in-domain SSL. Our control studies rule out pretraining dataset size as the bottleneck; rather, they point to task complexity. While SSL scales predictably on object-centric datasets like ImageNet (Figure 4), it struggles to capture the subtle, continuous radiographic features of OA (e.g., joint space narrowing, osteophytes) without semantic guidance. This contrasts with prior studies in other domains, such as chest radiography [21, 22], which notably reported substantial gains from in-domain pretraining.

We posit that this discrepancy is likely driven by differences in evaluation setup rather than domain characteristics alone. Unlike many previous works that utilize large, fixed validation sets even when training data is scarce, our protocol enforced proportional validation sampling and extensive Bayesian hyperparameter tuning for all methods, including the ImageNet baseline. Under these strictly controlled conditions, the performance gap narrows significantly. Our results suggest that standard ImageNet initialization is far more robust than typically credited in the medical SSL literature; when the supervised baseline is properly tuned, the marginal utility of learning pixel-level dependencies from in-domain datasets becomes negligible for classification tasks (both knee OA and chest tasks). Importantly, this negative result persists across additional image-only paradigms and data-diversity controls: mixed-domain medical pretraining (Knee+Chest) and masked autoencoder (MAE) pretraining do not consistently surpass ImageNet for KLG diagnosis (Appendix A–B).

Table 7

Prognosis Results (Structural Progression and Incidence). AUROC on OAI (Internal) and MOST (External). Multimodal SSL (ConVIRT) consistently outperforms ImageNet and Image-only SSL (MoCo, Barlow, ViCReg) across all data fractions, approaching the Supervised Upper Bound (KL Pret).

Approach	5% Data				10% Data				25% Data			
	OAI		MOST		OAI		MOST		OAI		MOST	
	LP	FT	LP	FT	LP	FT	LP	FT	LP	FT	LP	FT
Imgnet	0.514	0.581	0.532	0.604	0.539	0.580	0.566	0.599	0.546	0.618	0.575	0.645
MoCo	0.572	0.577	0.583	0.601	0.590	0.603	0.612	0.636	0.620	0.633	0.661	0.679
Barlow	0.543	0.550	0.565	0.566	0.577	0.589	0.602	0.608	0.586	0.632	0.618	0.669
ViCReg	0.565	0.545	0.576	0.558	0.583	0.586	0.600	0.615	0.598	0.653	0.612	0.689
CNN-JEPA	0.497	0.586	0.519	0.620	0.574	0.640	0.611	0.670	0.573	0.622	0.599	0.648
ConVIRT	0.628	0.629	0.676	0.658	0.640	0.655	0.693	0.701	0.656	0.673	0.709	0.722
GLORIA	0.626	0.596	0.651	0.630	0.638	0.638	0.671	0.658	0.641	0.666	0.679	0.703
<i>KL Pret (Sup)</i>	<i>0.650</i>	<i>0.679</i>	<i>0.692</i>	<i>0.724</i>	<i>0.691</i>	<i>0.694</i>	<i>0.742</i>	<i>0.745</i>	<i>0.689</i>	<i>0.716</i>	<i>0.739</i>	<i>0.766</i>

The introduction of radiology reports via Multimodal SSL (ConVIRT, GLORIA) revealed a fundamental interaction between pretraining data distribution and downstream task success. While we validated that ConVIRT yields significant gains for chest X-ray classification (Table 5), it failed to improve Knee KL grading, even though ConVIRT achieves significantly higher LP performance compared to ImageNet and other image-only SSL methods. We attribute this to the extreme spectrum bias inherent in tertiary care hospital data. Our analysis estimated that 93% of the uncurated pretraining cohort consisted of KL Grade 3 (pseudo labeled). Unlike chest radiography screening datasets (e.g., MIMIC-CXR), which contain a balance of normal and pathological findings, the knee hospital corpus is essentially a dataset of the sick. Lacking sufficient examples of healthy controls (KL 0/1) or early OA (KL 2), the model cannot learn the comparative features required for the full spectrum of diagnostic grading. Furthermore, radiology reports typically describe specific findings (e.g., "medial compartment narrowing") and do not have explicit KL grades, creating a semantic gap that multimodal objectives cannot easily bridge for this specific task.

Conversely, this biased dataset proved advantageous for prognosis. Predicting structural progression and incidence requires differentiating between patients who will remain stable and those who will deteriorate, a fine-grained discrimination task within the diseased population. Because the hospital pretraining data is heavily skewed toward symptomatic, diseased knees, the SSL objective is forced to learn robust representations of pathology variations. Consequently, ConVIRT pretrained on biased hospital data significantly outperformed ImageNet on structural progression/incidence prediction, approaching the performance of a supervised upper bound pretrained on expert KL grade labels.

Crucially, stratified analysis reveals that this advantage is not confined to the advanced disease population that dominated the pretraining set. As shown in our stratified results (Figure 6), multimodal pretraining consistently improved discrimination of progressors across *all* baseline severity

levels - including early-stage disease (KL 0/1) and established OA (KL 2/3). For instance, in the external validation cohort (MOST) at 10% labeled data, ConVIRT outperformed ImageNet even on the KL 0 (0.623 vs. 0.571) and KL 1 (0.584 vs. 0.545) subgroups. This finding is counter-intuitive; one might expect a model pretrained on majority KL 3 data to overfit to late-stage features. Instead, these results suggest that the visual features associated with symptomatic worsening in hospital patients, rely on fundamental structural changes that are universally relevant to prognosis, regardless of the starting disease stage.

These findings have significant implications for the development of medical AI. First, they suggest that the value of biased hospital data is task-dependent and beneficial for progressive diseases like knee OA. For diagnostic tasks requiring broad spectrum coverage, uncurated data may be detrimental; however, for prognostic tasks focused on disease evolution, the natural selection bias of hospital clinical data can be leveraged as a feature.

Second, our results demonstrate a scalable path for developing prognostic models. Validated prognostic datasets like OAI are small and expensive to curate. By leveraging readily available image-text pairs from hospital archives, we achieved performance competitive with fully supervised pretraining without requiring manual annotation. This approach could significantly reduce the cost of developing prognostic models for clinical trials and treatment selection.

Our study has several limitations. First, while the pretraining data (NYU) was large, it comes from a single medical center, potentially limiting geographic generalizability. Second, the OAI and MOST cohorts, which are derived from standardized research protocols, potentially lack the variability of routine clinical practice and therefore affecting generalizability to diverse care settings. They also lack racial diversity. As shown in Table 1, the OAI progression cohort is predominantly White (184 men, 253 women) compared to Black participants (26 men, 90 women). Similarly, the incidence cohort (Table 2) contains only 13 Black men compared to 133 White men. This imbalance may mask performance disparities across racial groups, and future work must validate these models on more diverse populations

to ensure equitable performance. Finally, we relied on 2D radiographs; while MRI provides higher sensitivity for early OA, radiographs remain the standard of care for initial assessment, ensuring the clinical relevance of our findings.

We conclude that while image-only self-supervision has limits in medical imaging, multimodal pretraining on uncured data offers a powerful mechanism for learning prognostic representations. By aligning the pretraining data distribution with the downstream clinical goal and leveraging the abundance of pathological examples in hospital records, we can build robust prognostic models that transcend the limitations of small, curated datasets.

5. Conclusions

In summary, we found that image-only self-supervised learning does not consistently outperform ImageNet pretraining for knee osteoarthritis diagnosis under rigorous finetuning, despite improvements in linear probing. In contrast, multimodal pretraining on uncured hospital radiographs paired with radiology impressions substantially improved prognostic modeling, including external validation on MOST. These findings show that the value of large-scale hospital data is strongly task-dependent: spectrum-biased routine-care image-text data may be poorly suited for learning general diagnostic severity graders, yet highly effective for prognosis when the downstream objective is aligned with the diseased population represented during pretraining. More broadly, this work highlights a scalable path toward building clinically useful prognostic models without requiring extensive manual annotation.

References

- [1] M. Cross, E. Smith, D. Hoy, S. Nolte, I. Ackerman, M. Fransen, L. Bridgett, S. Williams, F. Guillemin, C. L. Hill, et al., The global burden of hip and knee osteoarthritis: estimates from the global burden of disease 2010 study, *Annals of the rheumatic diseases* 73 (2014) 1323–1330.
- [2] V. Gulshan, L. Peng, M. Coram, M. C. Stumpe, D. Wu, A. Narayanaswamy, S. Venugopalan, K. Widner, T. Madams, J. Cuadros, et al., Development and validation of a deep learning algorithm for detection of diabetic retinopathy in retinal fundus photographs, *JAMA* 316 (2016) 2402–2410.
- [3] D. S. W. Ting, C. Y.-L. Cheung, G. Lim, G. S. W. Tan, N. D. Quang, A. Gan, H. Hamzah, R. Garcia-Franco, I. Y. San Yeo, S. Y. Lee, et al., Development and validation of a deep learning system for diabetic retinopathy and related eye diseases using retinal images from multiethnic populations with diabetes, *JAMA* 318 (2017) 2211–2223.
- [4] J. Irvin, P. Rajpurkar, M. Ko, Y. Yu, S. Ciurea-Ilcus, C. Chute, H. Marklund, B. Haghoo, R. Ball, K. Shpanskaya, et al., Chexpert: A large chest radiograph dataset with uncertainty labels and expert comparison, in: *Proceedings of the AAAI conference on artificial intelligence*, volume 33, pp. 590–597.
- [5] A. Esteva, B. Kuprel, R. A. Novoa, J. Ko, S. M. Swetter, H. M. Blau, S. Thrun, Dermatologist-level classification of skin cancer with deep neural networks, *Nature* 542 (2017) 115–118.
- [6] A. Tiulpin, J. Thevenot, E. Rahtu, P. Lehenkari, S. Saarakkala, Automatic knee osteoarthritis diagnosis from plain radiographs: a deep learning-based approach, *Scientific reports* 8 (2018) 1727.
- [7] B. Zhang, J. Tan, K. Cho, G. Chang, C. M. Deniz, Attention-based cnn for kl grade classification: Data from the osteoarthritis initiative, in: *2020 IEEE 17th international symposium on biomedical imaging (ISBI)*, IEEE, pp. 731–735.
- [8] J. H. Kellgren, J. Lawrence, et al., Radiological assessment of osteoarthritis, *Ann Rheum Dis* 16 (1957) 494–502.
- [9] A. Tiulpin, S. Klein, S. M. Bierma-Zeinstra, J. Thevenot, E. Rahtu, J. v. Meurs, E. H. Oei, S. Saarakkala, Multimodal machine learning-based knee osteoarthritis progression prediction from plain radiographs and clinical data, *Scientific reports* 9 (2019) 20038.
- [10] A. A. Tolpadi, J. J. Lee, V. Pedoia, S. Majumdar, Deep learning predicts total knee replacement from magnetic resonance images, *Scientific reports* 10 (2020) 6371.
- [11] H. R. Rajamohan, T. Wang, K. Leung, G. Chang, K. Cho, R. Kijowski, C. M. Deniz, Prediction of total knee replacement using deep learning analysis of knee mri, *Scientific reports* 13 (2023) 6922.
- [12] K. Leung, B. Zhang, J. Tan, Y. Shen, K. J. Geras, J. S. Babb, K. Cho, G. Chang, C. M. Deniz, Prediction of total knee replacement and diagnosis of osteoarthritis by using deep learning on knee radiographs: data from the osteoarthritis initiative, *Radiology* 296 (2020) 584–593.
- [13] H. R. Rajamohan, R. Kijowski, K. Cho, C. Deniz, A progressive risk formulation for enhanced deep learning based total knee replacement prediction in knee osteoarthritis, *Signal, Image and Video Processing* 19 (2025) 1–10.
- [14] T. Chen, S. Kornblith, M. Norouzi, G. Hinton, A simple framework for contrastive learning of visual representations, in: *International conference on machine learning*, PMLR, pp. 1597–1607.
- [15] X. Chen, H. Fan, R. Girshick, K. He, Improved baselines with momentum contrastive learning, *arXiv preprint arXiv:2003.04297* (2020).
- [16] J. Zbontar, L. Jing, I. Misra, Y. LeCun, S. Deny, Barlow twins: Self-supervised learning via redundancy reduction, in: *International conference on machine learning*, PMLR, pp. 12310–12320.
- [17] A. Bardes, J. Ponce, Y. LeCun, Vicreg: Variance-invariance-covariance regularization for self-supervised learning, *arXiv preprint arXiv:2105.04906* (2021).
- [18] M. Caron, H. Touvron, I. Misra, H. Jégou, J. Mairal, P. Bojanowski, A. Joulin, Emerging properties in self-supervised vision transformers, in: *Proceedings of the IEEE/CVF international conference on computer vision*, pp. 9650–9660.
- [19] A. Radford, J. W. Kim, C. Hallacy, A. Ramesh, G. Goh, S. Agarwal, G. Sastry, A. Askell, P. Mishkin, J. Clark, et al., Learning transferable visual models from natural language supervision, in: *International conference on machine learning*, PMLR, pp. 8748–8763.
- [20] J. Deng, W. Dong, R. Socher, L.-J. Li, K. Li, L. Fei-Fei, Imagenet: A large-scale hierarchical image database, in: *2009 IEEE conference on computer vision and pattern recognition*, Ieee, pp. 248–255.
- [21] H. Sowrirajan, J. Yang, A. Y. Ng, P. Rajpurkar, Moco pretraining improves representation and transferability of chest x-ray models, in: *Medical Imaging with Deep Learning*, PMLR, pp. 728–744.
- [22] S. Azizi, B. Mustafa, F. Ryan, Z. Beaver, J. Freyberg, J. Deaton, A. Loh, A. Karthikesalingam, S. Kornblith, T. Chen, et al., Big self-supervised models advance medical image classification, in: *Proceedings of the IEEE/CVF international conference on computer vision*, pp. 3478–3488.
- [23] Y. Zhang, H. Jiang, Y. Miura, C. D. Manning, C. P. Langlotz, Contrastive learning of medical visual representations from paired images and text, in: *Machine learning for healthcare conference*, PMLR, pp. 2–25.
- [24] S.-C. Huang, L. Shen, M. P. Lungren, S. Yeung, Gloria: A multimodal global-local representation learning framework for label-efficient medical image recognition, in: *Proceedings of the IEEE/CVF international conference on computer vision*, pp. 3942–3951.
- [25] H. Huang, S. Rawlekar, S. Chopra, C. M. Deniz, Radiology reports improve visual representations learned from radiographs, in: *Medical Imaging with Deep Learning*, PMLR, pp. 1385–1405.
- [26] M. Nevitt, D. Felson, G. Lester, The osteoarthritis initiative, *Protocol for the cohort study 1* (2006).
- [27] N. A. Segal, M. C. Nevitt, K. D. Gross, J. Hietpas, N. A. Glass, C. E. Lewis, J. C. Torner, The multicenter osteoarthritis study (most):

- opportunities for rehabilitation research, *PM & R: the journal of injury, function, and rehabilitation* 5 (2013) 10–1016.
- [28] A. E. Johnson, T. J. Pollard, S. J. Berkowitz, N. R. Greenbaum, M. P. Lungren, C.-y. Deng, R. G. Mark, S. Horng, *Mimic-cxr*, a de-identified publicly available database of chest radiographs with free-text reports, *Scientific data* 6 (2019) 317.
- [29] X. Wang, Y. Peng, L. Lu, Z. Lu, M. Bagheri, R. M. Summers, *Chestx-ray8: Hospital-scale chest x-ray database and benchmarks on weakly-supervised classification and localization of common thorax diseases*, in: *Proceedings of the IEEE conference on computer vision and pattern recognition*, pp. 2097–2106.
- [30] S. Datta, J. Posada, G. Olson, W. Li, C. O’Reilly, D. Balraj, J. Mesterhazy, J. Pallas, P. Desai, N. Shah, A new paradigm for accelerating clinical data science at stanford medicine, *arXiv preprint arXiv:2003.10534* (2020).
- [31] K. He, X. Zhang, S. Ren, J. Sun, Deep residual learning for image recognition, in: *Proceedings of the IEEE conference on computer vision and pattern recognition*, pp. 770–778.
- [32] A. Kalapos, B. Gyires-Tóth, *Cnn-jepa: Self-supervised pretraining convolutional neural networks using joint embedding predictive architecture*, in: *2024 International Conference on Machine Learning and Applications (ICMLA)*, IEEE, pp. 1111–1114.
- [33] M. Assran, Q. Duval, I. Misra, P. Bojanowski, P. Vincent, M. Rabbat, Y. LeCun, N. Ballas, Self-supervised learning from images with a joint-embedding predictive architecture, in: *Proceedings of the IEEE/CVF conference on computer vision and pattern recognition*, pp. 15619–15629.
- [34] S. Lee, Y. Kwon, N. Lee, K.-J. Bae, S. Park, Y. H. Kim, K.-H. Cho, et al., The prevalence of osteoarthritis and risk factors in the korean population: The sixth korea national health and nutrition examination survey (vi-1, 2013), *Korean Journal of Family Medicine* 40 (2018) 171.
- [35] T. Akiba, S. Sano, T. Yanase, T. Ohta, M. Koyama, *Optuna: A next-generation hyperparameter optimization framework*, in: *Proceedings of the 25th ACM SIGKDD international conference on knowledge discovery & data mining*, pp. 2623–2631.
- [36] K. He, X. Chen, S. Xie, Y. Li, P. Dollár, R. Girshick, Masked autoencoders are scalable vision learners, in: *Proceedings of the IEEE/CVF conference on computer vision and pattern recognition*, pp. 16000–16009.
- [37] E. Alsentzer, J. Murphy, W. Boag, W.-H. Weng, D. Jindi, T. Naumann, M. McDermott, Publicly available clinical bert embeddings, in: *Proceedings of the 2nd clinical natural language processing workshop*, pp. 72–78.
- [38] D. P. Kingma, Adam: A method for stochastic optimization, *arXiv preprint arXiv:1412.6980* (2014).
- [39] I. Loshchilov, F. Hutter, Decoupled weight decay regularization, *arXiv preprint arXiv:1711.05101* (2017).

A. Appendix - Extended Pretraining Analysis: Data Diversity and Domain Transfer

Building upon the main findings, we conducted further investigations to determine if the lack of improvement from image-only SSL was due to limited visual diversity in the knee radiograph dataset. We hypothesized that combining diverse medical domains (Knee + Chest) might learn more robust general-purpose features than knee data alone.

A.1. Methods Explored

We compared several additional SSL configurations:

- **Pretraining Data Variants:**

- **Knee Domain Mix:** The standard pretraining set (58k images) from OAI, MOST, and NYU.

- **Chest Domain:** Pretraining solely on NIH Chest X-ray 14.

- **Knee + Chest:** A combined pretraining dataset to test if visual diversity improves downstream transfer.

- **Evaluation:** We evaluated transfer performance on both the Knee KLG task (OAI) and the Chest pathology task (NIH/CheXpert) to assess cross-domain transferability.

A.2. Key Findings

As detailed in Tables A.1 and A.2, the results indicate that increasing visual diversity via domain mixing did not unlock performance gains:

- **Diversity did not replace Semantics:** The *Knee+Chest* models did not significantly outperform pure *Knee* models or *ImageNet* baselines on KLG grading (Table A.1).
- **Poor Cross-Domain Transfer:** Models pretrained on Chest X-rays performed poorly on Knee tasks, and vice-versa (Table A.2), confirming that pixel-level features are highly domain-specific and do not generalize well without semantic alignment.
- **ImageNet Baseline Strength:** ImageNet pretraining consistently rivaled or beat even the "diverse" medical pretraining (*Knee+Chest*), reinforcing that natural image features are a sufficiently robust starting point for medical tasks when fine-tuning is employed.

B. Appendix - Additional Image-Only SSL: Masked Autoencoders (MAE)

To further explore the potential of image-only self-supervised learning, we evaluated Masked Autoencoders (MAE), a generative approach that learns representations by reconstructing randomly masked patches of an image [36]. In these experiments, we use a **ViT-Small** encoder (following the standard MAE formulation) rather than the ResNet-34 backbone used in the main knee experiments; results are therefore reported as an additional control within this MAE-specific setup. Unlike contrastive methods (MoCo, Barlow Twins) which focus on global discrimination, MAE forces the model to learn local anatomical context.

B.1. Experimental Setup

We pretrained MAE models on the combined knee radiograph dataset, varying the masking ratio from 0.25 to 0.7. We evaluated these encoders on the KLG diagnosis task (OAI) and qualitatively assessed their reconstruction capabilities.

B.2. Results: The Reconstruction Paradox

The quantitative results (Table B.1) mirror our previous findings: MAE pretraining did not consistently outperform the ImageNet baseline. For instance, at 10% labeled data,

Table A.1

Extended KLG Diagnosis Results (OAI Test Set). Comparison of pretraining sources, including cross-domain (Chest) and mixed-domain (Knee+Chest) initialization. Adding Chest data to increase diversity (Knee+Chest) did not yield significant gains over ImageNet.

Pretraining Approach	1% Data		5% Data		10% Data	
	FT	LP	FT	LP	FT	LP
Random	0.397 (0.042)	0.200	0.555 (0.011)	0.200	0.619 (0.015)	0.200
Imgnet-pret	0.483 (0.040)	0.263	0.613 (0.014)	0.308	0.646 (0.009)	0.320
<i>In-Domain (Knee)</i>						
MoCo (Knee)	0.475 (0.050)	0.368	0.606 (0.010)	0.411	0.636 (0.012)	0.422
Barlow (Knee)	0.425 (0.063)	0.324	0.589 (0.018)	0.355	0.620 (0.010)	0.358
ViCReg (Knee)	0.471 (0.048)	0.336	0.585 (0.018)	0.374	0.635 (0.007)	0.373
<i>Cross-Domain (Chest)</i>						
Chest MoCo	0.283 (0.064)	-	0.563 (0.031)	-	0.611 (0.009)	-
Chest ViCReg	0.330 (0.050)	-	0.575 (0.010)	-	0.623 (0.007)	-
<i>Mixed-Domain (Knee+Chest)</i>						
Knee+Chest MoCo	0.363 (0.033)	-	0.577 (0.010)	-	0.636 (0.013)	-
Knee+Chest ViCReg	0.330 (0.050)	-	0.590 (0.014)	-	0.613 (0.009)	-

Table A.2

Extended Chest Pathology Results (NIH Test Set). Cross-domain evaluation showing that Knee pretraining fails to transfer effectively to Chest X-ray tasks compared to ImageNet.

Pretraining Approach	1% Data		5% Data		10% Data	
	FT	LP	FT	LP	FT	LP
Imgnet-pret	0.619 (0.013)	0.583	0.699 (0.011)	0.614	0.732 (0.009)	0.633
<i>In-Domain (Chest)</i>						
Chest MoCo	0.572 (0.015)	0.593	0.646 (0.012)	0.632	0.680 (0.004)	0.648
Chest Barlow	0.601 (0.018)	0.570	0.676 (0.006)	0.598	0.702 (0.006)	0.615
<i>Cross-Domain (Knee)</i>						
Knee MoCo	0.544 (0.015)	-	0.661 (0.010)	-	0.684 (0.010)	-
Knee ViCReg	0.551 (0.017)	-	0.654 (0.007)	-	0.668 (0.008)	-
<i>Mixed-Domain (Knee+Chest)</i>						
Knee+Chest MoCo	0.564 (0.008)	-	0.613 (0.010)	-	0.662 (0.008)	-
Knee+Chest Barlow	0.598 (0.010)	-	0.676 (0.007)	-	0.696 (0.010)	-

the best MAE model (masking ratio 0.5) achieved a balanced accuracy of 0.609, slightly underperforming ImageNet (0.618).

However, the qualitative analysis reveals a compelling paradox. As shown in Figure B.1, the MAE models successfully reconstructed high-fidelity anatomical details, including joint space and bone contours, even when 60% of the image was masked.

- **Anatomical Prior vs. Pathological Feature:** The high quality of reconstruction indicates the model learned a strong statistical prior of "healthy" knee anatomy. It can effectively "fill in" the missing pixels based on the general structure of a knee.
- **Diagnostic Failure:** Despite this understanding of structure, the downstream failure suggests that the features used for reconstruction (macroscopic geometry) are distinct from those required for diagnosis (subtle osteophytes, specific joint space narrowing patterns). The model learned to be an anatomical artist, but not a diagnostician.

C. Appendix - Implementation Details and Hyperparameters

To ensure reproducibility, we detail the specific architectures, initialization strategies, and the automated hyperparameter tuning protocol used in our experiments.

C.1. Model Architectures

We selected backbone architectures consistent with standard benchmarks in each respective domain:

- **Knee OA Experiments:** A **ResNet-34** backbone was used for all knee experiments (both image-only and multimodal) to match prior baselines in osteoarthritis grading.
- **Chest Radiography Experiments:** A **ResNet-50** backbone was used for all chest X-ray control experiments, consistent with standard evaluation protocols on CheXpert and NIH Chest X-ray 14.

Table B.1

Masked Autoencoder (MAE) Pretraining Results. Comparison of ImageNet pretraining vs. MAE pretraining with varying masking rates. Performance is reported as Balanced Accuracy (mean (std)) on the OAI test set. Despite successful image reconstruction, diagnostic performance remains stagnant.

Pretraining Approach	1% Data		5% Data		10% Data	
	FT	LP	FT	LP	FT	LP
Imgnet-pret	0.489 (0.052)	0.301 (0.017)	0.589 (0.013)	0.345 (0.013)	0.618 (0.013)	0.381 (0.010)
MAE 0.25	0.398 (0.098)	0.247 (0.011)	0.574 (0.012)	0.305 (0.005)	0.603 (0.011)	0.332 (0.005)
MAE 0.35	0.498 (0.024)	0.260 (0.011)	0.571 (0.012)	0.324 (0.006)	0.581 (0.021)	0.352 (0.005)
MAE 0.5	0.399 (0.095)	0.287 (0.013)	0.573 (0.007)	0.358 (0.012)	0.609 (0.009)	0.389 (0.012)
MAE 0.6	0.464 (0.066)	0.295 (0.012)	0.581 (0.017)	0.373 (0.015)	0.594 (0.012)	0.404 (0.017)
MAE 0.7	0.445 (0.050)	0.299 (0.015)	0.553 (0.011)	0.374 (0.015)	0.590 (0.011)	0.405 (0.015)

C.2. Pretraining Configuration

C.2.1. Image-Only SSL (MoCo, Barlow Twins, ViCReg)

We utilized the official reference implementations for each self-supervised method.

- **Training Schedule:** All image-only models were pre-trained for 100 epochs.
- **Optimization:** We utilized the default hyperparameter configurations provided in the official repositories, with the learning rate tuned specifically to achieve convergence on our datasets.

C.2.2. Multimodal SSL (ConVIRT, GLoRIA)

For image-text pretraining, we employed a transfer learning initialization strategy to accelerate convergence:

- **Image Encoder:** Initialized with standard ImageNet pretrained weights.
- **Text Encoder:** Initialized with **Bio_ClinicalBERT** [37] weights to leverage domain-specific medical language understanding.

C.3. Data Augmentation Pipeline

We utilized a consistent set of data augmentations during pretraining to encourage invariance to standard radiographic variations. The pipeline consisted of:

1. **Random Resized Crop:** Crops were resized to 224×224 pixels with a scale range of (0.5, 1.0).
2. **Gaussian Blur:** Applied with a probability of $p = 0.1$ and a radius $\sigma \in [0.1, 2.0]$.
3. **Random Horizontal Flip:** Applied with a probability of $p = 0.5$.
4. **Random Rotation:** Images were rotated by a random angle in the range $[-25^\circ, +25^\circ]$.

During finetuning Random Resized Crop, Random Horizontal Flip and Random Rotation were used. For evaluation, the input was resized to 256×256 and center cropped to 224×224 .

C.4. Downstream Fine-Tuning Protocol

For all downstream tasks, we utilized an automated Bayesian hyperparameter search rather than fixed settings. This was implemented using the **Optuna** framework with the following specific configuration:

C.4.1. Hyperparameter Search Space

For every unique combination of pretraining method (e.g., MoCo, ImageNet) and data fraction (1%, 5%, 10%), we ran 50 trials using a Tree-structured Parzen Estimator (TPE) sampler. The search space was defined as follows:

- **Optimizer:** Categorical selection between Adam [38], SGD, and AdamW [39].
- **Learning Rate (LR):** Log-uniform distribution in the range $[1e^{-6}, 1e^{-4}]$.
- **Weight Decay:** Log-uniform distribution in the range $[1e^{-6}, 1e^{-3}]$.
- **Training Epochs:** Integer range [40, 120].

C.4.2. Learning Rate Scheduling

We utilized a **One-Cycle Learning Rate Policy** for all fine-tuning runs to accelerate convergence. The maximum learning rate for the cycle was dynamically coupled to the base LR via a tunable multiplier:

$$LR_{max} = LR_{base} \times T_{mult} \quad (1)$$

where T_{mult} was a hyperparameter optimized in the integer range [1, 5].

C.4.3. Pruning Strategy

To improve search efficiency during Bayesian hyperparameter tuning, we employed a **Median Pruner**. Trials were terminated early if their validation accuracy at any epoch fell below the median of previous trials at the same step. A warmup period of 5 epochs was allowed before pruning began.

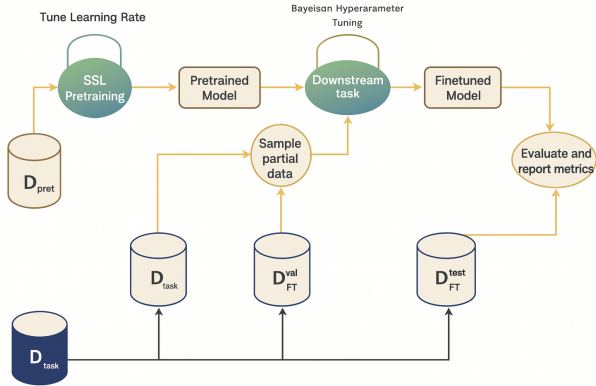


Figure 1: Overview of the Experimental Pipeline. The workflow consists of SSL pretraining followed by downstream fine-tuning. A critical feature of our protocol is the "Sample partial data" step: when evaluating low-data regimes (e.g., 1% training data), we proportionally subsample *both* the training and validation sets for hyperparameter tuning. This ensures a realistic evaluation, contrasting with prior works that utilize full validation sets even when training data is scarce.

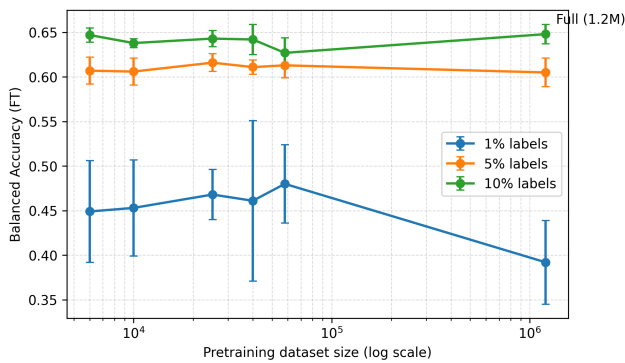


Figure 2: ImageNet scaling. Downstream KLG balanced accuracy on OAI versus ImageNet MoCo pretraining size (log-scale x-axis). Performance shows a plateau: reducing pretraining from 1.2M to 6k yields minimal changes, indicating that sheer natural-image scale does not resolve the medical task. Error bars denote reported standard deviations.

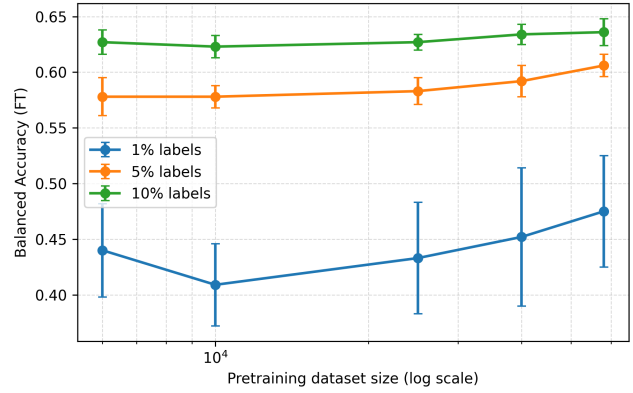


Figure 3: In-domain scaling (Fine-tuning). Downstream KLG balanced accuracy (FT) on OAI versus in-domain Knee MoCo pretraining size. Increasing in-domain pretraining data from 6k to 58k yields only marginal gains, consistent with a data-quality / signal bottleneck rather than data quantity. Error bars denote reported standard deviations.

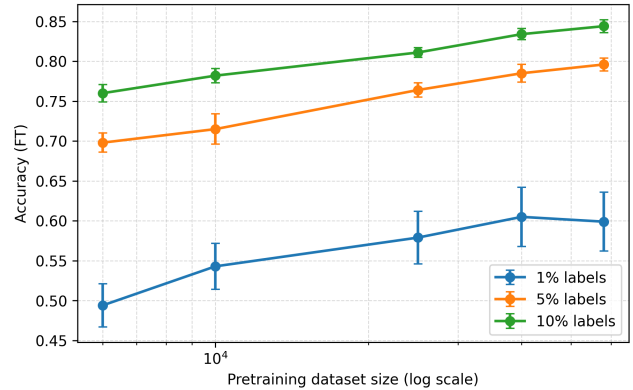


Figure 4: Control Experiment: Imagenette Scaling. Unlike the Knee domain, SSL (MoCo) shows strong, consistent scaling on simpler object-centric images (Imagenette). This confirms the difficulty lies in the medical task complexity, not the SSL method.

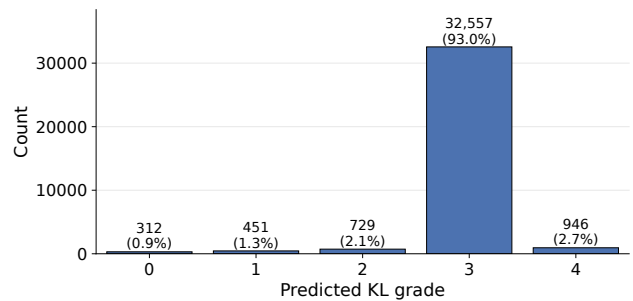


Figure 5: Selection Bias in Hospital Data. Distribution of inferred KL grades in the unlabeled pretraining cohort. Consistent with the study's inclusion criteria (patients with a clinical diagnosis of OA), the data is heavily skewed toward severe disease (93% KL 3), depriving the model of the healthy/early-stage examples needed to learn diagnostic grading.

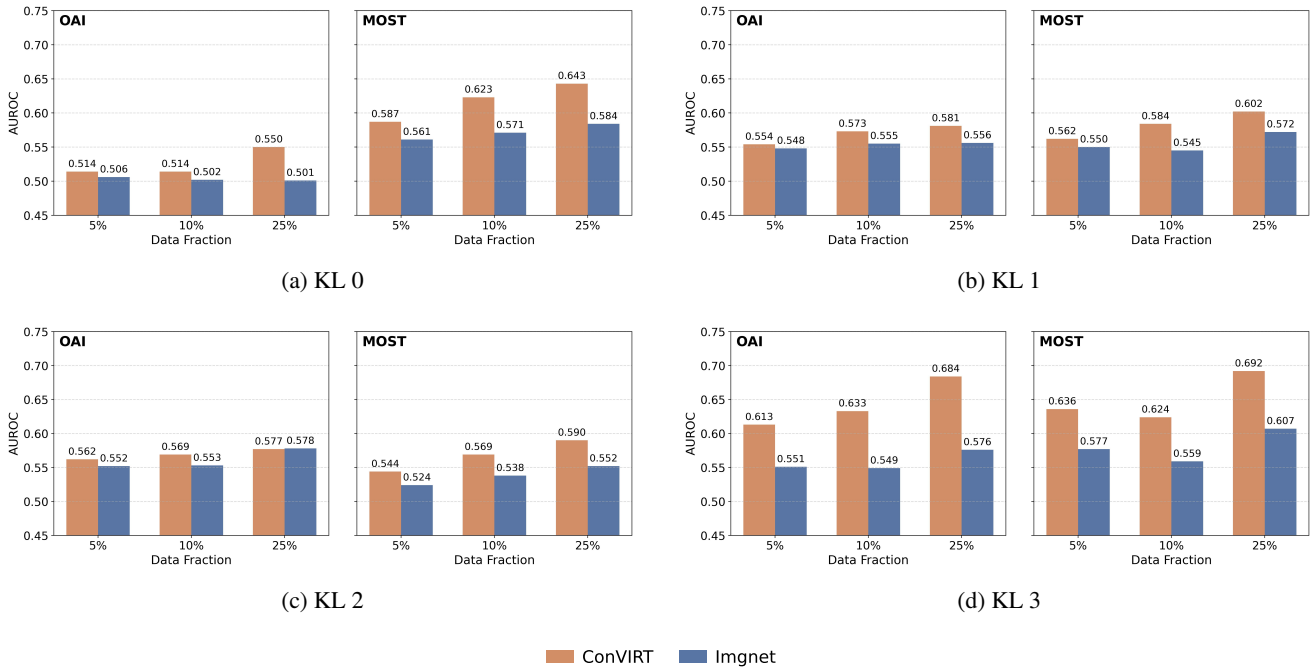


Figure 6: Stratified prognostic performance by baseline severity (ImageNet vs. ConVIRT). Performance (AUROC) on the structural progression/incidence task stratified by the baseline Kellgren-Lawrence (KL) grade of the knee. Despite the pretraining data being heavily skewed toward advanced disease (93% KL 3), the multimodal model (ConVIRT) consistently outperforms ImageNet across *all* severity strata in the external validation set (MOST). This indicates that the model learns generalized features of deterioration rather than overfitting to late-stage pathology.

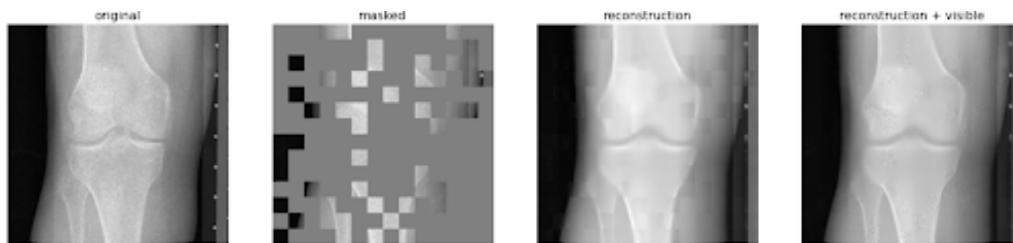


Figure B.1: The Reconstruction Paradox (MAE Visualizations). Sample reconstructions with a masking rate of 0.6, showing the original input, masked view, model reconstruction, and overlay. The model demonstrates high fidelity in hallucinating anatomical structures from partial data, yet this structural understanding did not translate to improved KLG diagnostic performance.